Submitted to the
International Europhysics Conference on High Energy Physics
July 17 - 23, 2003, Aachen, Germany

Abstract: 540 **Session: HP**

Dissociation of virtual photons in events with a leading proton at HERA

ZEUS Collaboration

Abstract

Dissociation of virtual photons, $\gamma^* p \to Xp$, has been studied at HERA with the ZEUS Leading Proton Spectrometer. The data cover photon virtualities $0.03 < Q^2 < 100$ GeV^2 and diffractive masses $1.5 < M_X < 70$ GeV. The cross section and the diffractive structure function $F_2^{D(3)}$ are presented as a function of Q^2. The dependence of $F_2^{D(3)}$ on β, the Pomeron momentum fraction probed by the photon, is also studied. The region investigated is extended over previously available results. The data are compared to predictions based on a saturation model.

1 Introduction

The diffractive dissociation of virtual photons, $\gamma^* p \to Xp$, can be investigated in the deep inelastic scattering (DIS) of electrons and protons at HERA by means of the reaction $ep \to eXp$, where the final-state proton carries a fraction of the incoming proton momentum close to unity. Seen from the proton rest frame, this reaction can be described in terms of the interaction of the hadronic fluctuation of the virtual photon with the proton via the exchange of an object with the vacuum quantum numbers; the hadronic fluctuation of the photon then dissociates into the hadronic state X. At the lowest order, the hadronic fluctuation is modeled by a quark-antiquark pair. Additional gluon radiation becomes important for large diffractive masses M_X. These $q\bar{q}$ and $q\bar{q}g$ dipole states have transverse dimensions which decrease as the photon virtuality, Q^2, increases. It is thus possible to study diffractive hadron-hadron interactions in a regime where one of the two interacting hadrons is so small that the strong interaction can be treated perturbatively. Alternatively, in the Breit frame, the reaction can be seen as the deep inelastic scattering of a pointlike virtual photon off the exchange object. This gives access to the partonic structure of the exchange and, in complete analogy with the usual DIS formalism for the proton structure function F_2, one can introduce a diffractive structure function F_2^D. In the language traditionally used in hadron-hadron physics [1], the exchange mediating the interaction is known as the Pomeron trajectory when the scattered proton has momentum equal, to within a few percent, to that of the incoming proton. For smaller values of the scattered proton momentum, the Reggeon and pion trajectories become important.

In this paper, the Q^2 dependence of the diffractive photon-proton cross section, $d\sigma^{\rm D}_{\gamma^* p}/dM_X$, is studied as a function of Q^2 for different values of the photon-proton centre-of-mass-energy, W. The data are also analysed in terms of the diffractive structure function, F_2^D, whose Q^2 and β dependences are investigated for different values of $x_{\IP}$, where β is the fraction of the Pomeron momentum probed by the exchanged photon and $x_{\IP}$ is the fraction of the proton momentum carried by the Pomeron.

The data belong to two different samples, hereafter referred to as the "low-Q^2 sample" and the "DIS sample". The former is restricted to the region $0.03 < Q^2 < 0.6$ GeV^2, $68 < W < 285$ GeV, $1.5 < M_X < 70$ GeV. The DIS sample is in the kinematic range $2 < Q^2 < 100$ GeV^2, $25 < W < 240$ GeV, $M_X > 1.5$ GeV. Events were selected by requiring the detection of the scattered proton in the ZEUS leading proton spectrometer (LPS), carrying a fraction x_L of the incoming proton momentum of at least 90%. This x_L range is sensitive to both Pomeron and Reggeon exchange.

2 Experimental method

The data used in this analysis were taken at the HERA ep collider in 1997 with the ZEUS detector and correspond to an integrated luminosity of 12.8 ± 0.2 pb^{-1} for the DIS sample and 3.6 ± 0.06 pb^{-1} for the low-Q^2 sample. At that time, HERA operated at a proton energy of 820 GeV and a positron energy of 27.5 GeV.

A detailed description of the ZEUS detector can be found elsewhere [2]. A brief outline of the components most relevant for this analysis is given below.

Charged particles are tracked by the central tracking detector (CTD) [3], which operates in a magnetic field of 1.43 T provided by a thin superconducting coil. The CTD consists of 72 cylindrical drift-chamber layers, organised in 9 superlayers covering the polar-angle[1] region $15^\circ < \theta < 164^\circ$. The relative transverse-momentum resolution for full-length tracks is $\sigma(p_t)/p_t = 0.0058 p_t \oplus 0.0065 \oplus 0.0014/p_t$, with p_t in GeV.

The high-resolution uranium-scintillator calorimeter (CAL) [4] consists of three parts: the forward (FCAL), the barrel (BCAL) and the rear (RCAL) calorimeters. Each part is subdivided transversely into towers and longitudinally into one electromagnetic section (EMC) and either one (in RCAL) or two (in FCAL and BCAL) hadronic sections (HAC). The smallest subdivision of the calorimeter is called a cell. The CAL relative energy resolutions, as measured under test-beam conditions, are $\sigma(E)/E = 0.18/\sqrt{E}$ for electrons and $\sigma(E)/E = 0.35/\sqrt{E}$ for hadrons (E in GeV).

Low-Q^2 events were selected by identifying and measuring the scattered positron in the beam-pipe calorimeter (BPC) and beam-pipe tracker (BPT) [5, 6]. The BPC was a tungsten-scintillator sampling calorimeter, located 3 m downstream of the interaction point and at a small angle to the positron beam direction. The BPT was a silicon-microstrip tracking device situated immediately upstream of the BPC. In 1997, it was equipped with two detector planes to measure the X coordinate.

The LPS [7] detected protons scattered at small angles in the proton direction and carrying a substantial fraction, x_L, of the incoming proton momentum; these particles remain in the beam-pipe and their trajectory was measured by a system of silicon-microstrip detectors very close (typically a few mm) to the proton beam. The track deflections induced by the magnets of the proton beam-line allowed a momentum analysis of the scattered proton. Resolutions better than 1% on the longitudinal momentum and 5 MeV

[1] The ZEUS coordinate system is a right-handed Cartesian system, with the Z axis pointing in the proton-beam direction, referred to as the "forward direction", and the X axis pointing left towards the centre of HERA. The coordinate origin is at the nominal interaction point. The pseudorapidity is defined as $\eta = -\ln(\tan\frac{\theta}{2})$, where the polar angle, θ, is measured with respect to the proton-beam direction.

on the transverse momentum have been achieved. The effective transverse-momentum resolution is, however, dominated by the intrinsic transverse-momentum spread of the proton beam at the interaction point, which is about 40 MeV in the horizontal plane and about 90 MeV in the vertical plane.

3 Kinematics and cross section

In the low-Q^2 analysis, the kinematic variables Q^2 and W and the inelasticity y, the fraction of energy lost by the electron in the proton rest frame, were determined from the energy, E'_e, and the angle, θ_e, of the scattered positron ("electron method") measured in the BPC/BPT.

In the DIS analysis the identification of the scattered positron was based on a neural network algorithm [8] which uses information from the CAL. The variables W and Q^2 were reconstructed with a combination of the electron method and the double angle method [9].

The energy deposit in the CAL and the track momenta of the charged particles were clustered into objects called "energy-flow objects" (EFOs). Each of them is regarded as a particle [10,11]. The mass M_X of the diffractive system X was calculated from the EFOs.

The momentum of the scattered protons detected in the LPS, p^{LPS}, was measured together with its component perpendicular (parallel) to the beam direction, p_T^{LPS} (p_Z^{LPS}). From these quantities, the fractional momentum of the scattered proton, x_L, and the square of the four-momentum exchanged at the proton vertex, t, were determined as:

$$x_L = p_Z^{LPS}/E_p;$$

$$t = -\frac{(P_T^{LPS})^2}{x_L}.$$

The diffractive-variables $x_{\mathbb{P}}$ and β represent respectively the proton momentum fraction carried by the Pomeron and the Pomeron momentum fraction probed by the photon. They were calculated as:

$$x_{\mathbb{P}} = \frac{M_X^2 + Q^2}{W^2 + Q^2};$$

$$\beta = \frac{Q^2}{Q^2 + M_X^2}.$$

The cross section, $\sigma^{\mathrm{D}}_{\gamma^* p}$, for the diffractive dissociation of virtual photons, $\gamma^* p \to Xp$, is related to the cross section for the process $ep \to eXp$ by

$$\frac{d\sigma^{\rm D}_{\gamma^* p}}{dM_X} = \frac{\pi Q^2 W}{\alpha(1+(1-y)^2)} \cdot \frac{d^3\sigma^{\rm D}_{ep}}{dQ^2 dW dM_X}.$$

The diffractive structure function is related to the diffractive cross section by

$$\frac{d\sigma^D_{ep}}{d\beta dQ^2 dx_{\rm I\!P}} = \frac{4\pi\alpha^2}{\beta Q^4}[1-y+\frac{y^2}{2(1+R^{D(4)})}]F_2^{D(4)}(\beta, Q^2, x_{\rm I\!P}, t),$$

where $R^{D(4)}$ is the ratio of the cross sections for longitudinally and trasversely polarised photons, and was assumed to be zero for this analysis. The diffractive structure function $F_2^{D(3)}$ is obtained by integrating $F_2^{D(4)}$ over t.

4 Monte Carlo simulation

In the low-Q^2 analysis the reaction $ep \to eXp$ was simulated with the Monte Carlo (MC) generator EPSOFT2.0 [10,12,13]. The Triple-Regge formalism [1] was used to parametrise the cross section.

In the DIS analysis the same reaction was modelled with RAPGAP [14], which is based on the factorisable model of Ingelman and Schlein [15]. The diffractive structure function $F_2^{D(4)}$ was expressed as a sum of a Pomeron and a secondary Reggeon contribution [16].

QED radiative effects were simulated through HERACLES [17]. The measurements of the diffractive structure function and of the diffractive cross section presented hereafter are corrected for these effects.

All generated events were passed through the standard ZEUS detector simulation, based on the GEANT3.13 program [18], and the trigger-simulation package.

5 Results

5.1 Q^2 dependence of the cross section

Figure 1 shows the diffractive cross section, $d\sigma^{\rm D}_{\gamma^* p}/dM_X$, as a function of Q^2 at different M_X and W values. The present measurement is shown together with the previous ZEUS result [10] corrected for the residual double-dissociative background. The contribution from the background was assumed to be 31% [10].

The present results extend the previous ZEUS measurements [10, 11, 19] to a wider, so far unexplored kinematic region, and notably reach higher values of M_X, lower values of

Q^2 as well as values of W close to the kinematic limit. The data exhibit a behaviour qualitatively similar to that of the total photon-proton cross section [20]: the diffractive cross section falls rapidly with Q^2 at high Q^2; conversely, as $Q^2 \to 0$, the cross section dependence on Q^2 becomes very weak.

The main features of the data are broadly reproduced by a fit based on the BEKW model [19, 21]. This model parametrizes the diffractive cross section in terms of fluctuations of transversely and longitudinally polarised virtual photons either into $q\bar{q}$ or $q\bar{q}g$ states. In the kinematic domain of the present measurement the contribution from longitudinally polarised photons can be neglected. The β (and hence M_X) spectra of the dipole states are determined by general properties of the photon wave-function, with the $q\bar{q}$ contribution to the cross section proportional to $\beta(1-\beta)$ and the $q\bar{q}g$ contribution proportional to $(1-\beta)^\gamma$. The $q\bar{q}$ component has no Q^2 dependence, while the $q\bar{q}g$ component has a logarithmic Q^2 dependence of the type $\log(1+\mathrm{Q}^2/\mathrm{Q}_0^2)$, where the scale parameter Q_0^2 is taken to be 0.4 GeV^2. The model assumes that the cross sections of the two components have a power-like behaviour in $x_{\mathbb{P}}$ of the type $(x_0/x_{\mathbb{P}})^{n(Q^2)}$, where the x_0 parameter is taken to be 0.01. In the fit, the $x_{\mathbb{P}}$ dependence was obtained from the data, along with the relative normalisation of the $q\bar{q}$ and $q\bar{q}g$ contributions and the coefficient γ. The fit was limited to the region $x_{\mathbb{P}} < 0.01$, where Pomeron exchange dominates. For small values of M_X the $q\bar{q}$ states dominate in the DIS region, while at large masses the $q\bar{q}g$ contribution becomes dominant. Going from the DIS region to the low-Q^2 region, for a given value of M_x, β also decreases, and again the $q\bar{q}g$ contribution becomes dominant.

The similarity of the behaviour of the diffractive and total cross sections is emphasized by Fig. 2, where the ratio of the diffractive cross section to the total virtual photon proton cross section, $(M_X^2 d\sigma^{\mathrm{D}}_{\gamma^* p}/dM_X)/\sigma^{\mathrm{tot}}_{\gamma^* p}$, is presented as a function of Q^2 at different M_X and W values. The values of the $\gamma^* p$ cross section were obtained from the ALLM97 parametrization [22]. At low values of Q^2, the Q^2 dependence of the diffractive cross section is similar to that of $\sigma^{\mathrm{tot}}_{\gamma^* p}$. In the DIS regime, in the region $Q^2 \gg M_X^2$, $d\sigma^{\mathrm{D}}_{\gamma^* p}/dM_X$ decreases with Q^2 more rapidly than $\sigma^{\mathrm{tot}}_{\gamma^* p}$, while for $Q^2 \ll M_X^2$ the ratio increases with Q^2. Here again, the results for $x_{\mathbb{P}} < 0.01$ are well reproduced by the BEKW fit.

5.2 Diffractive structure function

The diffractive structure function was evaluated under the assumption that $R^{D(4)} = 0$.

The dependence of the diffractive structure function on Q^2 is presented in Fig. 3 for different values of $x_{\mathbb{P}}$ and β. The diffractive structure function rises with Q^2 in all the available kinematic region. These positive scaling violations presumably reflect a large gluonic contribution in the diffractive exchange. The behaviour is similar in all $x_{\mathbb{P}}$ bins, both in the Pomeron dominated region and at larger $x_{\mathbb{P}}$, where Reggeons become

important. The results are compared with the prediction of the saturation model [23]. In this model [24], diffractive DIS is described as the interaction of the $q\bar{q}$ ($q\bar{q}g$) fluctuation of the virtual photon with the proton. The parameters of the $q\bar{q}$ and $q\bar{q}g$ dipole cross sections were obtained from a fit to the F_2 data. The latest modification of the model [23] includes the QCD DGLAP evolution of the gluon distribution. In the region of applicability of the model, $x_{I\!P} < 0.01$, the Q^2 dependence of the data is well described, although the data points are higher than the model prediction, an effect which becomes stronger at low values of β.

Figure 4 shows some of the points of Fig. 3 along with the low-Q^2 data. As for the proton structure function F_2, conservation of the electromagnetic current requires that $F_2^D \propto Q^2$ for $Q^2 \to 0$, a trend supported by the present data.

The dependence of the diffractive structure function on β, presented in Fig. 5 for different values of $x_{I\!P}$ and Q^2, has a very different behaviour at different values of $x_{I\!P}$, presumably reflecting the different partonic structure of the exchange probed. Here again the results are well described by the prediction of the saturation model.

6 Summary

The diffractive dissociation of virtual photons, $\gamma^* p \to Xp$, has been studied at HERA over a wide $x_{I\!P}$ and Q^2 region.

The Q^2 dependence of the diffractive cross section has been measured: while at low Q^2 the data do not exhibit a strong Q^2 dependence, at larger Q^2 the cross section falls rapidly for increasing Q^2. This change of behaviour is qualitatively similar to that observed in the $\gamma^* p$ cross section, as confirmed by the Q^2 dependence of the ratio of the diffractive to the total cross section.

The diffractive structure function rises with Q^2 both in the Pomeron dominated region and at larger $x_{I\!P}$. The β dependence of $F_2^{D(3)}$ has instead a very different behaviour at different values of $x_{I\!P}$.

The main features of the data are well described both by a parametrisation based on the BEKW [21] model and by the prediction of the saturation model [23]. This indicates that dipole models including $q\bar{q}$ ad $q\bar{q}g$ contributions are suitable to describe diffractive processes in ep collisions from the low-Q^2 region to the DIS regime. The data suggest the increasing importance of the $q\bar{q}g$ states at low Q^2.

7 Acknowledgements

We thank the DESY Directorate for their strong support and encouragement, and the HERA machine group for their diligent efforts. We are grateful for the support of the DESY computing and network services. The design, construction and installation of the ZEUS detector have been made possible by the ingenuity and effort of many people from DESY and home institutes who are not listed as authors. It is also a pleasure to thank K. Golec-Biernat for providing the prediction of his model for the kinematic range covered by our data.

References

[1] P.D.B. Collins, *An introduction to Regge Theory and High Energy Physics*, Cambrige University Press, Cambrige (1977).

[2] ZEUS Collab., U. Holm (ed.), *The ZEUS Detector,* Status Report (unpublished), DESY (1993);
`http://www-zeus.desy.de/bluebook/bluebook.html` .

[3] N. Harnew et al., Nucl. Instr. and Meth. **A279**, 290 (1989);
B. Foster et al., Nucl. Phys. Proc. Suppl. **B32**, 181 (1993);
B. Foster et al., Nucl. Inst. and Meth. **A338**, 254 (1994).

[4] M. Derrick et al., Nucl. Instr. and Meth. **A309**, 77 (1991);
A. Andresen et al., Nucl. Instr. and Meth. **A309**, 101 (1991);
A. Caldwell et al., Nucl. Instr. and Meth. **A321**, 356 (1992);
A. Bernstein et al., Nucl. Instr. and Meth. **A336**, 23 (1993).

[5] T. Monteiro, PhD Thesis, Hamburg University (1998), DESY-Thesis-1998-027;
B. Surrow, PhD Thesis, Hamburg University (1998), DESY-Thesis-1998-004;
J. Tickner,PhD Thesis, Oxford University (1997), RAL-TH-97-018.

[6] C. Amelung, PhD Thesis, Bonn University (1999), BONN-IR-99-14 and DESY-Thesis-2000-002.

[7] ZEUS Collaboration, M. Derrick et al., Z. Phys. **C73**, 253 (1997).

[8] H. Abramowicz, A. Caldwell and R. Sinkus, Nucl. Instr. and Meth. **A356**, 508 (1995).

[9] S. Bentvelsen, J. Engelen and P. Kooijman, *Reconstruction of (x,Q^2) and extraction of structure functions in neutral current scattering at HERA, Proc. Workshop on Physics at HERA*, W. Buchmuller and G. Ingelman (eds.), Vol. 1, p. 23, DESY (1992).

[10] ZEUS Collaboration, J. Breitweg et al., Eur. Phys. J. **C6**, 43 (1999).

[11] G. Briskin, PhD Thesis, Tel Aviv University (1998), DESY-Thesis-1998-036.

[12] M. Kasprzak, PhD Thesis, Warsaw University (1996), DESY F35D-96-16.

[13] M. Inuzuka, PhD Thesis, Tokyo University (1999), KEK Report 99-9.

[14] H. Jung, Comp. Phys. Comm. **86**, 147 (1995).

[15] G. Ingelmann and P.E. Schlein, Phys. Lett. **B152**, 256 (1985).

[16] H1 Collaboration, C. Adloff et al., Z. Phys. **C76**, 613 (1997).

[17] K. Kwiatkowski, H. Spiesberger and H.-J. Möhring, Comput. Phys. Commun. **69** 155 (1992).

[18] GEANT 3.13, R. Brun et al., CERN DD/EE/84-1 (1987).

[19] ZEUS Collaboration, S. Chekanov et al., Eur.Phys. J. **C25**, 169 (2002).

[20] ZEUS Collaboration, J. Breitweg et al., Phys. Lett. **B487**, 53 (2000).

[21] J.Bartels et al., Eur. Phys. J. **C7**, 443 (1999).

[22] H. Abramowicz and A. Levy, Preprint DESY-97-251 (hep-ph/9712415), DESY (1997).

[23] J. Bartels, K. Golec-Biernat and H. Kowalski, Phys. Rev. **D66**, 014001 (2002).

[24] K. Golec-Biernat and M. Wusthoff, Eur. Phys. J. **C20**, 313 (2001).

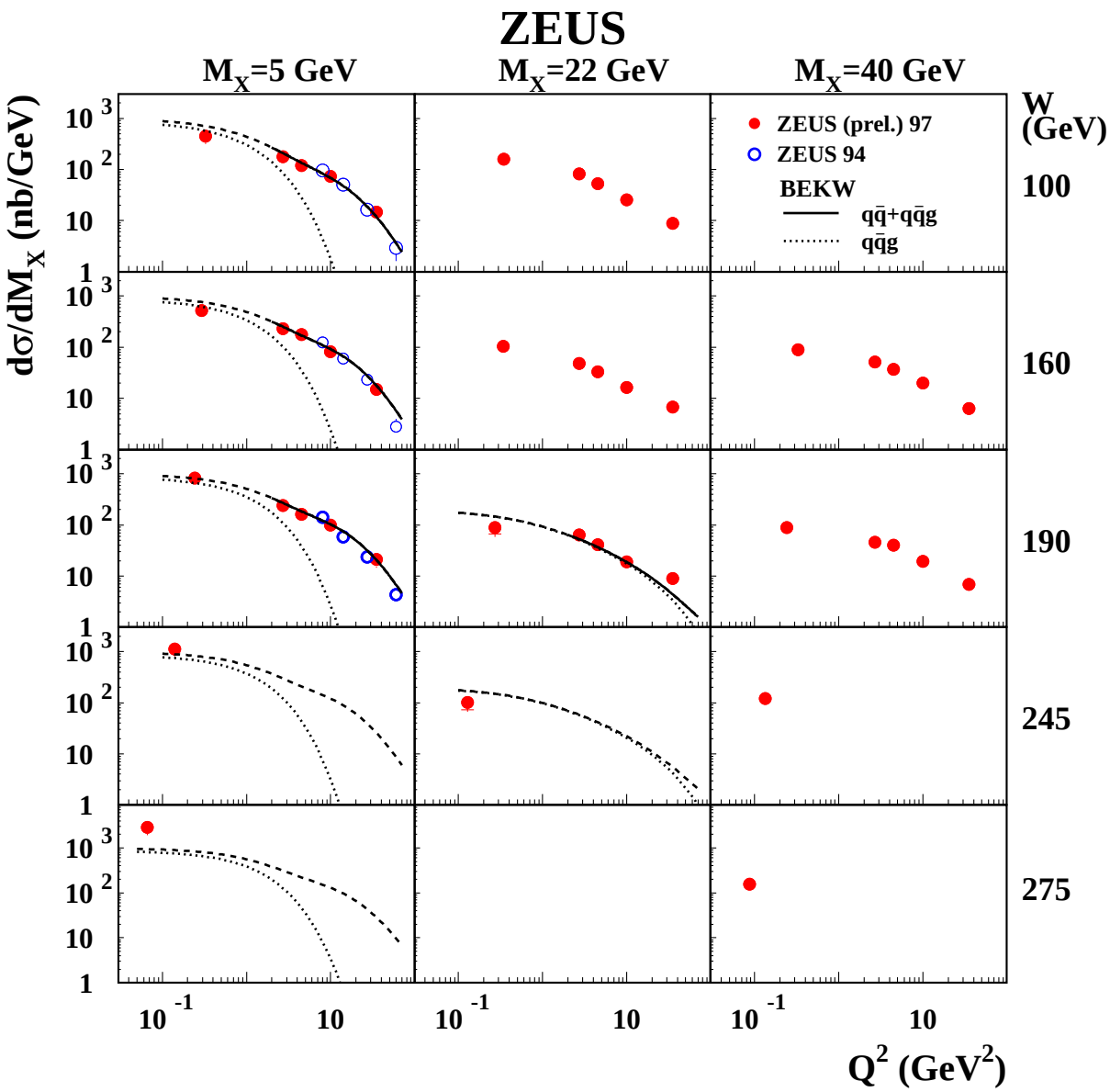

Figure 1: *The diffractive cross section $d\sigma^{\mathrm{D}}_{\gamma^* p}/dM_X$ as a function of Q^2 at different W and M_X values. The inner error bars show the statistical uncertainties and the full bars are the statistical and the systematic uncertainties added in quadrature. The overall normalisation uncertainty of $\sim 10\%$ is not shown. The solid (dashed) lines are the results of the BEKW fit (extrapolation of the BEKW fit) described in the text. The dotted lines are the results of the same fit for the $q\bar{q}g$ contribution alone.*

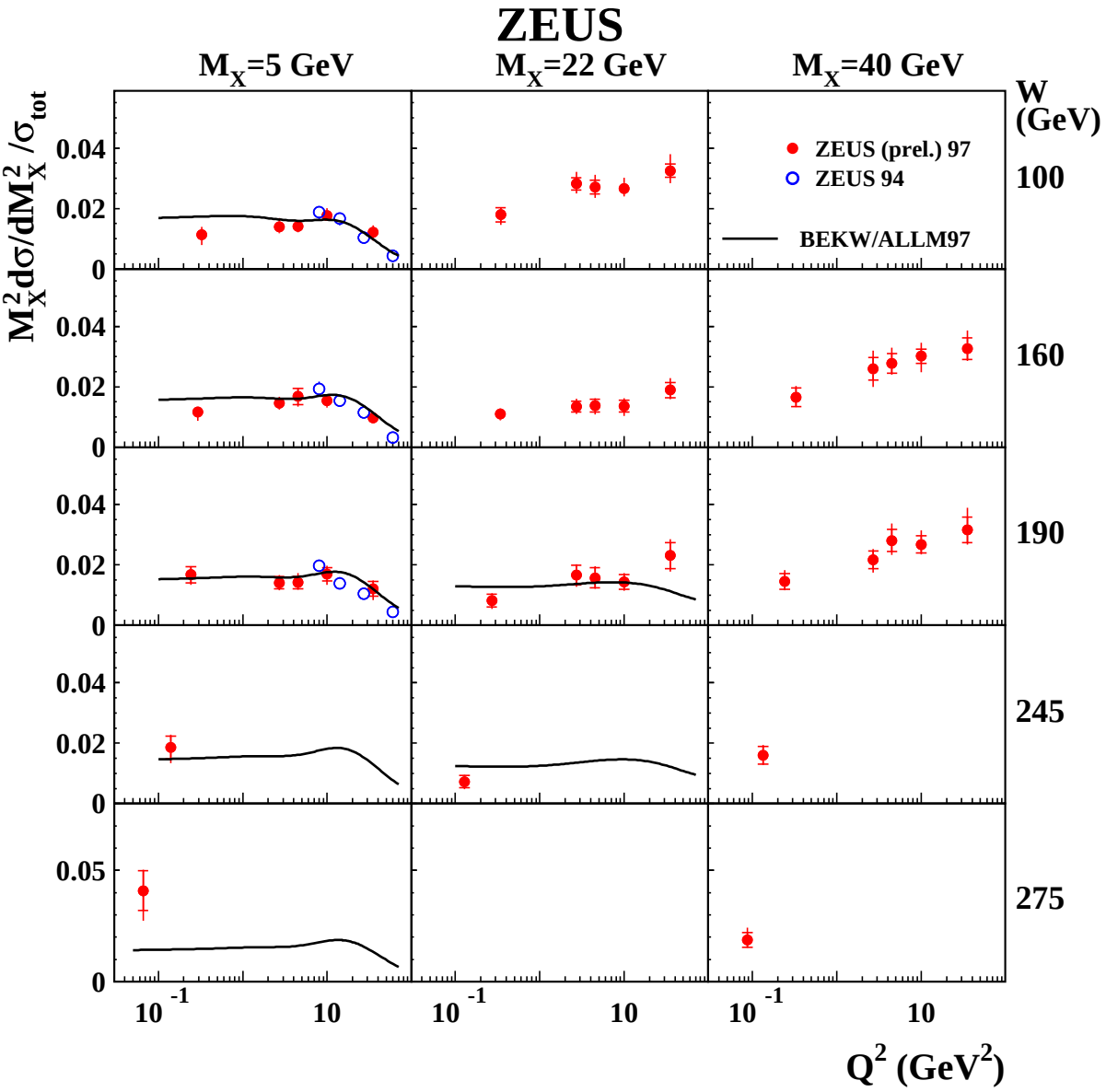

Figure 2: *The ratio of the diffractive cross section to the total virtual photon proton cross section as a function of Q^2 at different W and M_X values. The inner error bars show the statistical uncertainties and the full bars are the statistical and the systematic uncertainties added in quadrature. The overall normalisation uncertainty of $\sim$ 10% is not shown. The solid lines are the result of the BEKW fit described in the text.*

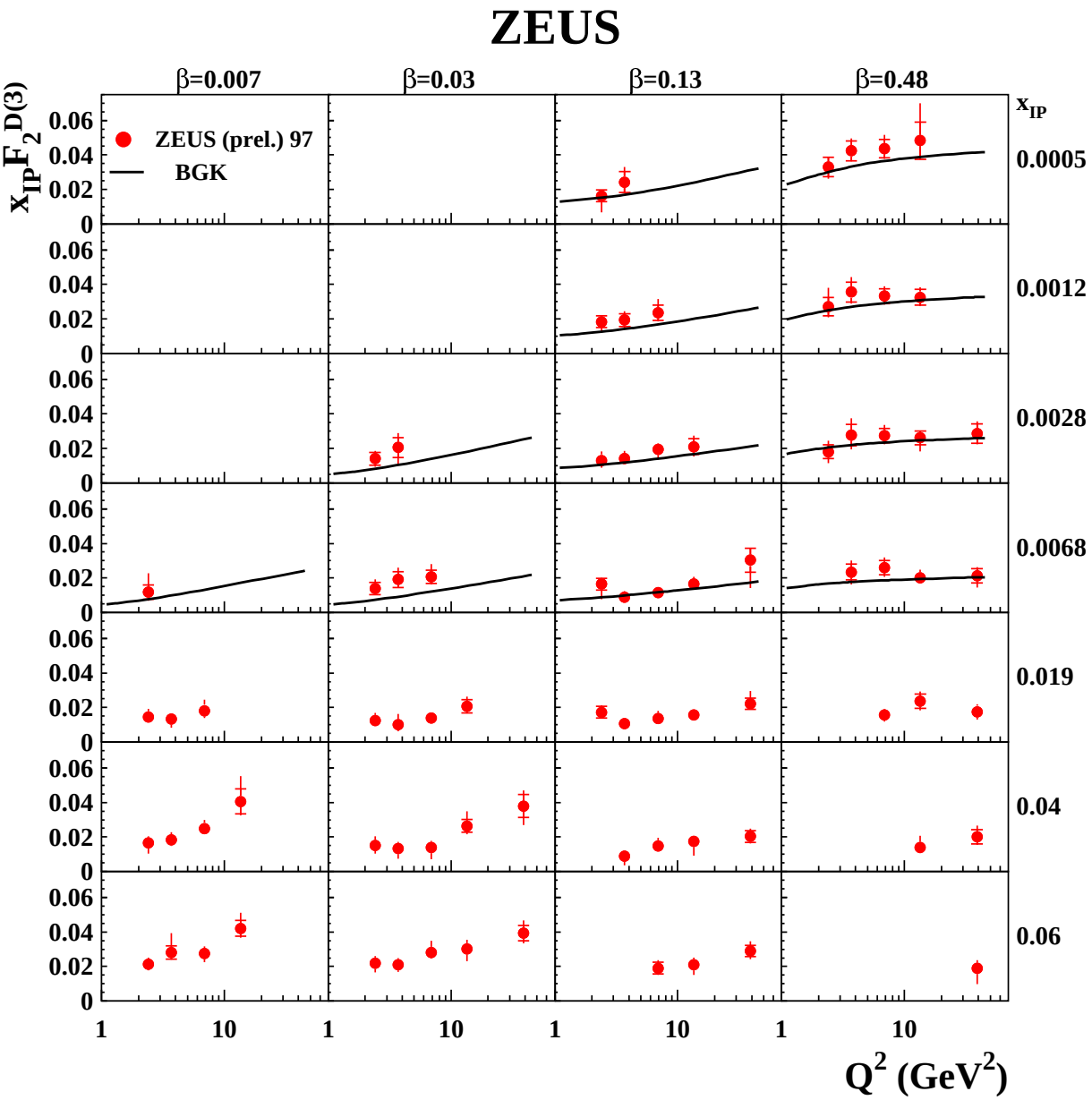

Figure 3: *The diffractive structure function multiplied by $x_{\mathbb{P}}$, $x_{\mathbb{P}}F_2^{D(3)}$, as a function of Q^2, for different values of $x_{\mathbb{P}}$ and β. The inner error bars show the statistical uncertainties and the full bars are the statistical and the systematic uncertainties added in quadrature. The overall normalisation uncertainty of $\sim$ 10% is not shown. The solid lines are the prediction of the saturation model described in the text.*

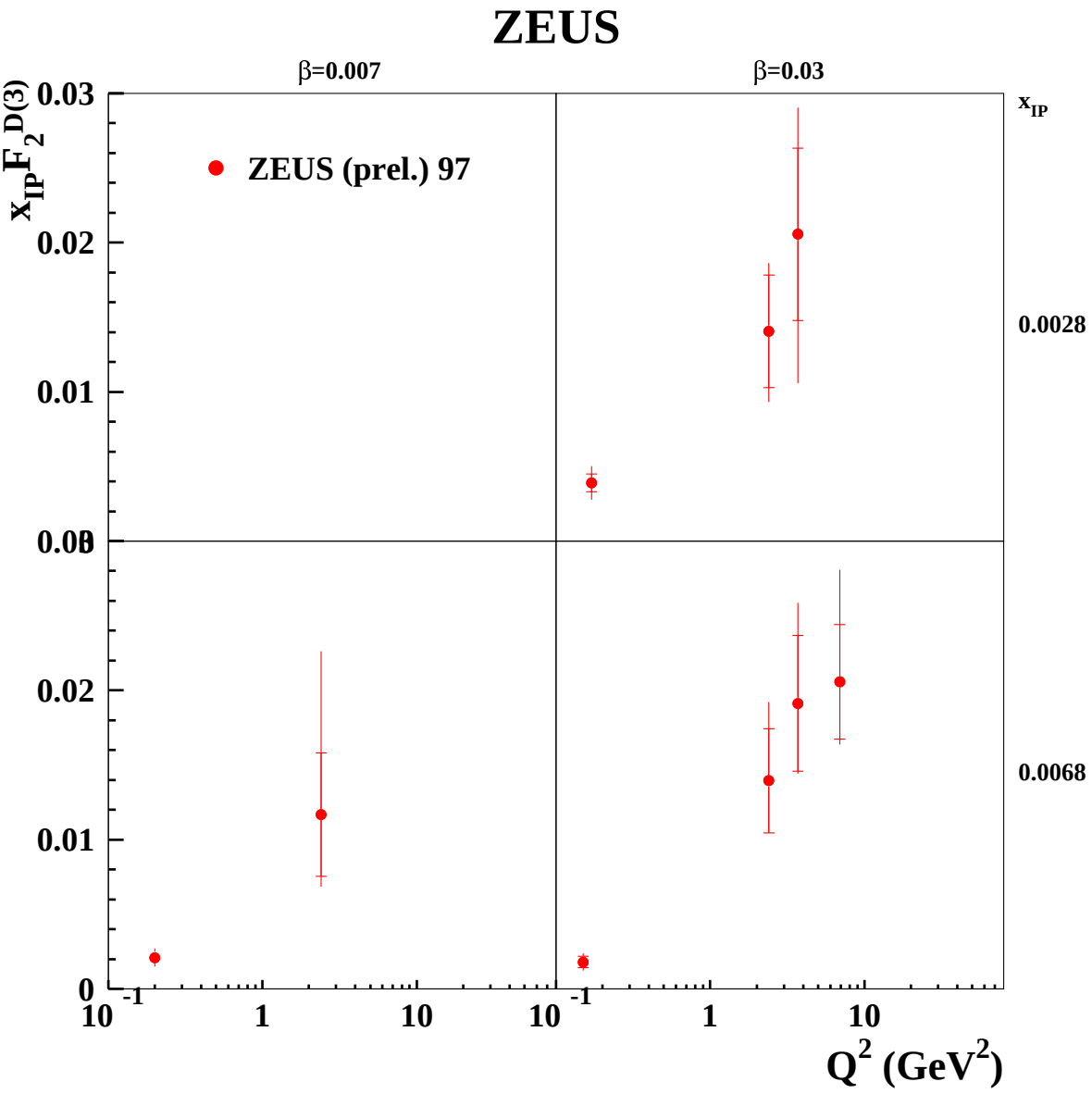

Figure 4: *The diffractive structure function multiplied by $x_{\mathbb{P}}$, $x_{\mathbb{P}} F_2^{D(3)}$, as a function of Q^2, for different values of $x_{\mathbb{P}}$ and β. The inner error bars show the statistical uncertainties and the full bars are the statistical and the systematic uncertainties added in quadrature. The overall normalisation uncertainty of $\sim 10\%$ is not shown.*

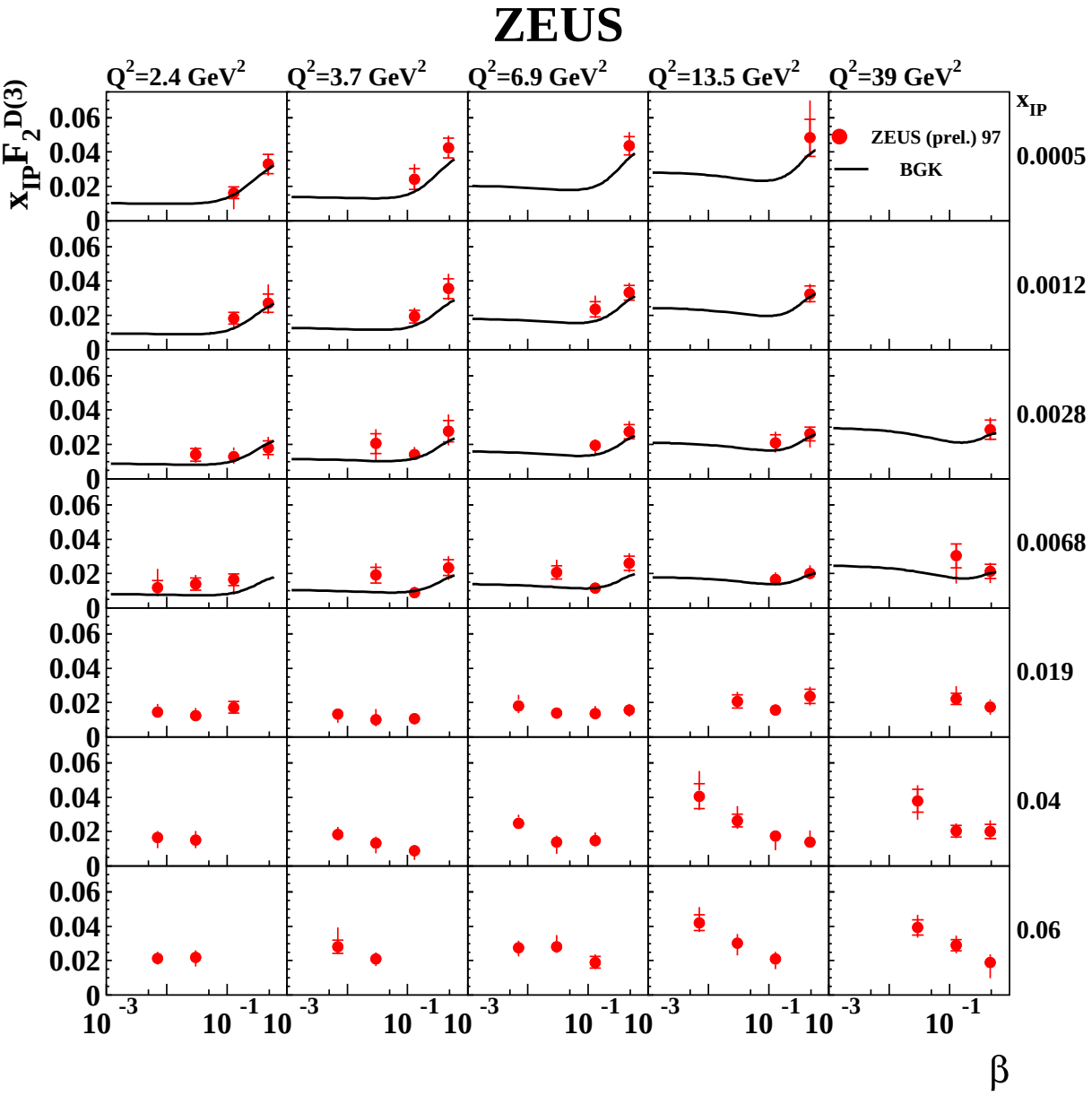

Figure 5: *The diffractive structure function multiplied by $x_{\mathbb{P}}$, $x_{\mathbb{P}}F_2^{D(3)}$, as a function of β, for different values of $x_{\mathbb{P}}$ and Q^2. The inner error bars show the statistical uncertainties and the full bars are the statistical and the systematic uncertainties added in quadrature. The overall normalisation uncertainty of $\sim$ 10% is not shown. The solid lines are the prediction of the saturation model described in the text.*